PERGAMON

Aerosol Science 34 (2003) 1347–1370

Journal of
Aerosol Science

www.elsevier.com/locate/jaerosci

Transmission electron microscopical and aerosol dynamical characterization of soot aerosols

M. Wentzel[a], H. Gorzawski[b], K.-H. Naumann[c], H. Saathoff[c], S. Weinbruch[b,*]

[a] *Fachgebiet Verbrennungskraftmaschinen, Fachbereich Maschinenbau, Technische Universität Darmstadt, Petersenstr. 30, 64287 Darmstadt, Germany*

[b] *Umweltmineralogie, Institut für Angewandte Geowissenschaften, Technische Universität Darmstadt, Schnittspahnstr. 9, 64287 Darmstadt, Germany*

[c] *Forschungszentrum Karlsruhe, Institut für Meteorologie und Klimaforschung, Postfach 3640, 76021 Karlsruhe, Germany*

Received 12 November 2001; accepted 2 June 2003

Abstract

Size, morphology and microstructure of Palas soot, Diesel soot and of Diesel soot/ammonium sulfate mixtures were studied by transmission electron microscopy (TEM). The diameter of the primary particles derived from TEM is 6.6 ± 1.7 nm for Palas soot and 22.6 ± 6.0 nm for Diesel soot. Palas soot predominantly consists of amorphous carbon. In a few cases, nanocrystalline graphite with domain sizes on the order of 1 nm were observed. Primary particles of Diesel soot always show an onion-shell structure of nanocrystalline graphite with domain sizes between 2–3 nm. Fractal properties of 37 Diesel soot agglomerates were determined from TEM images by two different techniques. The average fractal dimension of Diesel soot derived from TEM is 1.70 ± 0.13. TEM further showed that the initially external mixture of Diesel soot and ammonium sulfate developed with time in a significant degree of internal mixing.

A second independent approach to determine the fractal properties of soot is based on computer simulations of the aerosol dynamics. A good reproduction of the time evolution of mass and number concentrations and of the mobility size distribution was achieved. The primary particle diameters obtained from the computer simulations (7.3 ± 0.8 nm for Palas soot, 25 ± 3 nm for Diesel soot) are in excellent agreement with the TEM results. The fractal dimension of Diesel soot received from the COSIMA algorithm of 1.9 ± 0.2 (overlap of primary particles was taken into consideration) is consistent with the value obtained from TEM image analysis. For Palas soot, the computer simulation yielded a fractal dimension of 2.0 ± 0.1 (overlap was not corrected, as the overlap coefficient is not known).

* Corresponding author. Tel.: +49-6151-165280; fax: +49-6151-164021.
E-mail address: dh6d@hrzpub.tu-darmstadt.de (S. Weinbruch).

0021-8502/$ - see front matter © 2003 Elsevier Ltd. All rights reserved.
doi:10.1016/S0021-8502(03)00360-4

1. Introduction

Soot is an important component of most atmospheric aerosols, with fossil fuel and biomass burning being the major anthropogenic sources (e.g., Cachier, 1998; Cooke, Liousse, Cachier, & Feichter, 1999). The optical properties of soot are of particular interest due to the high absorption efficiency. On a global scale, the direct radiative forcing of soot is estimated to be $+0.2$ W/m^2 (IPCC, 2001). However, this number critically depends on the mixing state with other aerosol constituents. For example, it has recently been shown (Jacobson, 2001) that the mixing state of soot in atmospheric aerosols approaches an internal mixture leading to a much higher positive forcing on the order of $+0.5$ to $+0.6$ W/m^2. This result implies that soot may be the second most important component (after carbon dioxide) of global warming in terms of direct forcing (Jacobson, 2001).

As the mixing state is a key parameter in estimating the radiative forcing of soot, studies of the aerosol dynamics and mixing are of great importance. In this contribution we report the results of a combined transmission electron microscopy (TEM) and computer simulation study conducted within the framework of the AIDA soot characterization campaign 1999.

Soot particles freshly emitted from Diesel engines or aircraft combustors often exhibit ramified and apparently irregular agglomerate structures. As a result, their aerosol dynamical and optical properties differ significantly from those of compact spheres. Since in a statistical sense the volume structure of soot agglomerates is often characterized by self-similarity over several orders of magnitude in size (e.g., Sorensen & Feke, 1996; Köylü, Faeth, Farias, & Carvalho, 1995a), the fractal dimension D_f plays a central role in describing the geometrical, optical, and aerodynamical behavior of these particles.

Principally, this important parameter can be inferred from the analysis of two-dimensional electron microscopic images even for three-dimensional structures as long as $D_f < 2$. Unfortunately, in practise this approach has usually been plagued with difficulties due to finite size effects, primary particle overlap and screening effects, and to cluster anisotropy (e.g., Tence, Chevalier, & Jullien, 1986; Oh & Sorensen, 1997; Katrinak, Rez, Perkes, & Buseck, 1993). In a recent paper, however, Brasil, Farias, and Carvalho (1999) devised a semi-empirical scheme which promises to overcome at least part of the problems encountered so far. By correlating the structural properties of computer simulated three-dimensional agglomerates of well-defined geometries with those of their two-dimensional projections, they were able to derive simple recipes for extracting the value of D_f and other relevant parameters such as the fractal prefactor k_g from electron micrographs.

The second route towards determining the fractal parameters of soot agglomerates considered in our study relies on the comparison of measured and simulated time evolutions of mass and number concentrations and of the mobility equivalent size distribution of airborne particles. Model studies using the fractal–aerosol behavior code COSIMA indicated that the rates of aerosol dynamical processes like diffusion, sedimentation, and coagulation are especially sensitive to structural changes associated with small variations of D_f (Naumann, 2003; Naumann & Bunz, 1992; Möhler, Naumann, & Schöck, 1994). Furthermore, trajectories calculated for different values of D_f diverge strongly with time. In the AIDA chamber of the Research Centre Karlsruhe (Saathoff et al., 2003), predicted and observed mass concentration half-lives are more than a week for Diesel soot and about 2 weeks for particles generated by spark discharge between graphite electrodes (Palas soot), respectively, under ambient conditions, slightly depending on the initial mass and number concentrations. Therefore, it was easily possible to extend our aerosol dynamical experiments over time ranges ensuring a

high susceptibility to analysis by model calculations. Besides being of interest for comparative and cross-validation purposes, the structural parameters for Diesel and Palas soot derived from TEM image analysis and from the computer simulation approach also provided the basis for the interpretation of the aerosol optical measurements conducted during the AIDA soot characterization campaign as outlined and discussed in the companion paper by Schnaiter et al. (2003).

2. Experimental

2.1. Sampling and transmission electron microscopy

Samples were collected on Ni or Cu TEM grids with conducting Formvar foil using a three-stage cascade impactor (Wieser & Wurster, 1986). The 50% cut-off diameters of the three impactor stages are 0.18–0.35, 0.35–0.65, and 0.65–1.2 μm. At a flow rate of 0.5 l/min, the sampling time was 2s. To avoid alteration, samples were not coated with carbon prior to TEM analysis.

TEM was performed with two different instruments: a Philips CM12, operated at 120 kV, and for high resolution imaging a Philips CM 20 (with an ultra-twin lens), operated at 200 kV. For chemical analysis, both instruments are equipped with an energy-dispersive X-ray detector (Si(Li)). The TEM images were digitized with a scanner using a resolution of 300 dpi. The image processing software Optimas (version 6.1) was used for fractal analysis. We provide results from experiments #2, #5 and #6 (pure Diesel soot and mixtures of Diesel soot with ammonium sulfate). The numbering of the experiments refers to the introductory paper by Saathoff et al. (2003), which also describes the standard aerosol characterization techniques relevant to this study. The resolution and contrast achieved on Palas soot (experiments #1 and #3) was not sufficient to determine the fractal dimension reliably. The size and the microstructure of Palas soot given in this paper is not obtained from samples of the AIDA campaign but from exploratory experiments. However, as the same soot generator (operated under the same conditions) was used, it can be assumed that the size and microstructure of Palas soot of these samples are also characteristic for the AIDA campaign.

2.2. Fractal analysis of TEM images

Soot agglomerates usually consist of small primary particles that coagulate to form irregular clusters. The complex geometry of these agglomerates can be described as mass fractals with the following relationship between the number of primary particles of an agglomerate N_p and the radius of gyration R_g (e.g., Forrest & Witten, 1979; Köylü, Xing, & Rosner, 1995b):

$$N_p = k_g \left(\frac{R_g}{r_p} \right)^{D_f} \tag{1}$$

with r_p the mean primary particle radius, D_f the fractal dimension and k_g the fractal pre-factor.

It should be noticed in this context that the aggregates do not fulfill the requirements for fractals in a mathematical sense. However, the term has been used by several authors (see, e.g., Köylü et al., 1995b; Brasil et al., 1999, and references therein) to characterize fractal-like agglomerates.

There are several approaches (e.g., Katrinak et al., 1993; Kaye, 1994; Huang, Turpin, Piho, Kittelson, & McMurry, 1994; Köylü et al., 1995b; Brasil et al., 1999; Dye, Rhead, & Trier, 2000;

Mikhailov, Vlasenko, Krämer, & Niessner, 2001) to determine the fractal properties of aerosol agglomerates from two-dimensional projections (e.g., TEM-images). The nested squares method is the most commonly used technique for fractal analysis of individual aerosol aggregates (e.g., Forrest & Witten, 1979; Tence et al., 1986; Samson, Mulholland, & Gentry, 1987; Zhang, Sorensen, Ramer, Olivier, & Merklin, 1988; Lesaffre, 1989; Katrinak et al., 1993; Huang et al., 1994). In this approach, a series of concentric square boxes is placed on each aggregate. Then, the number of pixels inside the square that contains a part of the agglomerate N_{sq} and the length l_{sq} (in pixels) are determined for each square. The fractal dimension can be obtained from a double-logarithmic plot of N_{sq} versus l_{sq}. In this plot, the slope of a straight line fitted to the data is equal to the fractal dimension. The least-squares fit was calculated using a weighting factor of $N_{sq}^{-0.5}$ (e.g., Forrest & Witten, 1979; Katrinak et al., 1993). In many papers, the fractal analysis of aerosol aggregates is limited to the determination of the fractal dimension. However, it was shown by several authors (e.g., Wu & Friedlander, 1993; Cai, Lu, & Sorensen, 1995; Köylü et al., 1995b; Oh & Sorensen, 1997) that both the fractal dimension and the fractal pre-factor must be known accurately in order to characterize the fractal geometry of an aggregate completely. Unfortunately, the fractal pre-factor cannot be determined by the nested squares method, as this approach is based on the number of pixels (i.e., the size of the pixels is not considered). The fractal dimension obtained by the nested squares method depends on the orientation of the agglomerates in the image, on the location of the center of the squares and on the distribution of the primary particles around the center of mass of the aggregate. For example, during our analysis we have observed variations up to 20% for the fractal dimension when analyzing objects with known fractal properties in different orientations. In addition, the nested squares method does not take into account the partial overlapping of primary particles of an agglomerate, which is frequently observed in atmospheric aerosols. According to Tence et al. (1986), the nested squares method systematically underestimates the true fractal dimension due to the finite size of the aggregates. The magnitude of this error is about 0.3 for aggregates with a true fractal dimension close to $D_f = 2$.

A promising method to deduce the fractal properties of an assembly of aggregates from two-dimensional projections was published recently by Brasil et al. (1999). Details of this approach will not be repeated here. However, it is appropriate to outline some fundamentals. The geometrical properties required for the characterization of the agglomerates, that can be measured from projected images, are the primary particle mean diameter d_p, the mean overlap coefficient $C_{ov} = (d_p - d_{ij})/d_p$ (with d_{ij} the distance between two touching particles), the projected maximum length of an agglomerate L_a, and the projected area of the agglomerate A_a. The projected maximum length of an agglomerate L_a may be used as a substitute of the radius of gyration R_g, as the latter is not easily obtained from image analysis. In this case, the following relation is used to infer the fractal properties of the agglomerates:

$$N_p = k_L \left(\frac{L_a}{d_p} \right)^{D_f L} \tag{2}$$

with D_{fL} and k_L the fractal dimension and fractal pre-factor based on the projected maximum length. Using the algorithm of Brasil et al. (1999), the following properties can be inferred for each individual agglomerate: number of primary particles N_p, radius of gyration R_g, and total exposed surface area S_a. The fractal dimension D_f and the fractal pre-factor k_g can be obtained from the analysis of several agglomerates. It should be emphasized here that the fractal dimension D_f and the fractal

pre-factor k_g are obtained from an ensemble of agglomerates, i.e. both parameters are statistical in nature. The parameters D_{fL} and k_L are derived from a double logarithmic plot of the number of primary particles N_p versus the normalized projected maximum length L_a/d_p (Eq. (2)). The slope of a straight line fitted to the data represents the fractal dimension D_{fL}, the intercept yields the fractal pre-factor k_L. According to Brasil et al. (1999), the fractal parameters D_f and k_g (which are based on the radius of gyration) can then be calculated as follows:

$$D_f = D_{fL}, \tag{3}$$

$$k_g = k_L * (1.5)^{D_f}. \tag{4}$$

Alternatively, the fractal dimension D_f and the fractal pre-factor k_g may be obtained directly from a double logarithmic plot of N_p versus R_g/r_p (Eq. (1)). For this purpose, the radius of gyration R_g may be estimated, to a first approximation, from the projected maximum length L_a (Brasil et al., 1999):

$$\frac{L_a}{2 * R_g} \cong 1.50. \tag{5}$$

In general, the radius of gyration depends on the fractal dimension D_f:

$$\frac{L_a}{2 * R_g} = \sqrt{\frac{D_f + 2}{D_f}}. \tag{6}$$

However, the errors introduced by the approximation of Eq. (5) are small for the range of fractal dimensions encountered in this study and can, therefore, be neglected.

The recipe developed by Brasil et al. (1999) is based on the analysis of computer-simulated agglomerates with known properties. The parameters used to construct the agglomerates in the computer simulation ($N_p \leqslant 512; 0 \leqslant C_{ov} \leqslant 0.33; D_f = 1.78; 1.5 \leqslant k_L \leqslant 3.1$) are similar to those observed in our study. Thus, the application of the method of Brasil et al. (1999) should lead to reliable results.

There are several reasons why we favor the approach of Brasil et al. (1999) for the determination of fractal properties. First, we are not primarily interested in describing the morphological properties of individual agglomerates. Instead, we want to study the dynamical behavior of the aerosol and want to infer the agglomeration mechanism. For this purpose, a method which derives fractal properties from a number of agglomerates is more appropriate, as it covers a larger size range and reduces the statistical errors compared to the analysis of individual aggregates. Second, the uncertainties of analyzing individual agglomerates (e.g., variable orientation in the image, inhomogeneous distribution of primary particles around the center of mass, partial overlapping of primary particles) are avoided. Third, the nested squares method does not take care of the limitations that arise from the fact that two-dimensional projections are studied. Fourth, the fractal pre-factor k_g, which is required to characterize the geometry of the agglomerates completely, cannot be obtained by the nested squares method. For comparison, however, the fractal dimension of individual agglomerates determined by the nested squares method is also given.

2.3. Fractal analysis of combined size distribution and mass concentration measurements

Alternatively, the average fractal dimension of agglomerate aerosols may be determined by simultaneous mobility sizing and mass concentration measurements using the formalism outlined in Naumann (2003). Combining Eqs. (4) and (21) of Naumann (2003) and rearranging results in the following relation between the mass equivalent radius R_m and the mobility equivalent radius R_{me}:

$$\frac{R_m}{r_{\mathrm{p}}} = \left\{ \left[\frac{R_{\mathrm{me}}}{(-0.06483 D_{\mathrm{f}}^2 + 0.6353 D_{\mathrm{f}} - 0.4898) r_{\mathrm{p}}} \right]^{D_{\mathrm{f}}} \frac{1}{f} \right\}^{1/3}. \tag{7}$$

The volume filling factor f accounts for the fact that even in a most closely packed structure of spheres of equal size the primary particles cannot occupy more than about 74% of the available volume. It is related to k_{g} by

$$f = \frac{1}{k_{\mathrm{g}}} \left(\frac{D_f + 2}{D_{\mathrm{f}}} \right)^{D_{\mathrm{f}}/2}. \tag{8}$$

Based on Eq. (7), size distributions measured with a scanning mobility particle sizer (DMA 3071 & CNC 3010, TSI) were converted to respective size distributions related to the mass equivalent diameter. Weighting with particle mass and integrating over all sizes yielded an estimate of the mass concentration which could be compared to the one measured by coulometric analysis (Coulomat 702, Ströhlein) of quartz fiber filter samples (MK 360, Munktell). With f already fixed to 1.43 for nonoverlapping monomers (Naumann, 2003; Naumann & Bunz, 1991) and r_{p} available from our TEM images D_{f} remained the only variable parameter in this procedure and could, therefore, be determined uniquely. Please note that Eq. (7) is strictly valid only under continuum regime conditions. Considering transition regime or free molecular cases, it has to be supplemented by a suitable Cunningham-type correction as discussed in Section 2.2 of Naumann (2003).

It has been exemplified in Naumann (2003) that dynamical processes in agglomerate aerosols such as diffusion, coagulation, and sedimentation are highly sensitive to small variations of D_{f}. A less pronounced but still significant dependence is also observed with respect to the primary particle radius r_{p}. Therefore, the intercomparison of measured and numerically simulated time evolutions of mass and number concentrations as well as mobility-based size distributions provides a second theoretically supported route towards determining D_{f} and r_{p} simultaneously which does not require the recording of TEM images. For our analysis the sectional aerosol behavior code COSIMA (Naumann, 2003; Naumann & Bunz, 1992) was employed which simulates the structural and dynamical properties of airborne agglomerate particles using a formalism based on statistical mechanics and fractal scaling laws. Specifically, the code accounts for hydrodynamic interactions and shielding of the primary particles inside a cluster within the framework of the Kirkwood–Riseman theory (Kirkwood & Riseman, 1948; Doi & Edwards, 1986). For a detailed description of the formalism and the code validation see Naumann (2003). All simulations were initialized with experimentally determined size distributions measured immediately after homogeneous mixing of the aerosol had been established in the AIDA chamber. Subsequently D_{f} and r_{p} were varied for optimum agreement between experimental and numerical results.

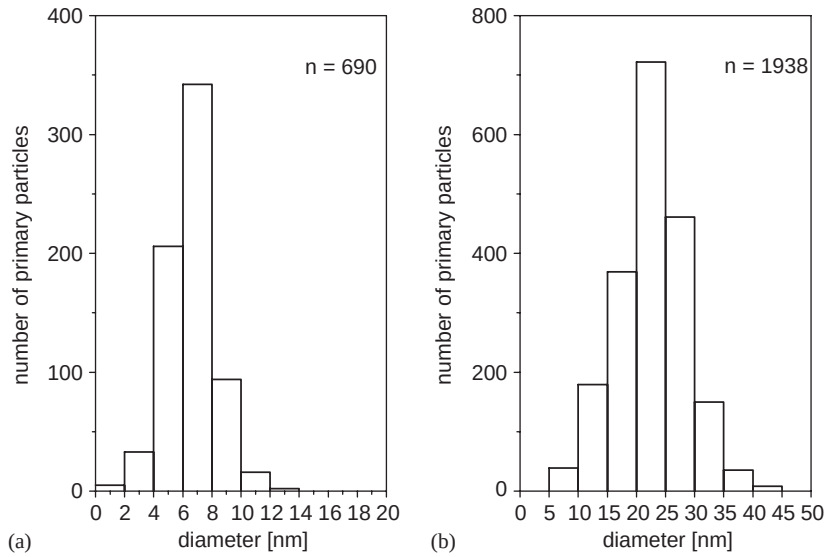

Fig. 1. Size distribution of primary particles of Palas soot (a) and Diesel soot (b) determined by TEM.

3. Results and discussion

3.1. Size, microstructure, and chemical composition of soot primary particles

The size and the microstructure of primary particles of Palas soot and of Diesel soot were studied by TEM. The size distributions of primary particles are given in Fig. 1. From the TEM analysis of the 1938 Diesel soot primary particles their average diameter was determined to 22.6 ± 6.0 nm. Unfortunately, the samples taken during experiment #2 after 3 h and during experiment #6 after 44h show a systematic trend towards larger values compared to all others (see Table 1). Since the reason for this deviation is not yet clear, we have to accept, for the time being, the accordingly enhanced error margin of our result. The primary particles of Palas soot are much smaller (6.6 ± 1.7 nm; $n=690$) than those of Diesel soot. The microstructure of primary particles was studied by high-resolution imaging (Figs. 2 and 3). Palas soot consists of amorphous carbon (Fig. 2b) or in a few cases of nanocrystalline graphite (Fig. 2c). In the amorphous regions only short-range ordering (on the order of one graphite (0 0 1) lattice plane) is encountered. The nanocrystalline primary particles have the typical onion-shell structure (Fig. 2c) described for atmospheric soot (e.g., Seinfeld & Pandis, 1998; Buseck & Posfai, 1999; Posfai, Anderson, & Buseck, 1999; Posfai & Molnar, 2000). The domain size is on the order of 1 nm (3 graphite (0 0 1) lattice planes). We do not have any evidence that the nanocrystalline structure observed in a few primary particles of Palas soot formed under electron bombardment in the instrument. Primary particles of Diesel soot always show the onion-shell structure (Fig. 3a). With approximately 7–10 graphite (0 0 1) lattice planes (Fig. 3b), the domain sizes are much larger compared to Palas soot.

In the energy-dispersive X-ray spectra (Fig. 4) of both, Palas and Diesel soot, a silicon peak is observed besides the dominating carbon peak. The presence of small amounts of silicon in the

Table 1
Properties of individual Diesel soot agglomerates derived from TEM using the approach of Brasil et al. (1999)

Exp. #	Time (h)	Agglomerate	L_a (nm)	d_p (nm)[a]	C_{ov}	N_p
2	3	973	914	48 ± 8.4	0.15	209
		978	794	38 ± 7.5	0.14	423
		979	1914	39 ± 6.0	0.12	1260
		981	754	45 ± 10.0	0.19	190
		b613	184	37 ± 2.9	0.13	28
		b617	218	41 ± 6.7	0.14	33
		b618	357	34 ± 7.3	0.12	89
2	45	c087	91	24 ± 2.3	0.29	11
		c146	423	22 ± 4.3	0.12	288
		c148	728	20 ± 3.8	0.13	570
		c153	223	20 ± 3.0	0.16	116
		c156	429	21 ± 3.2	0.11	122
5	3	b142	248	21 ± 5.1	0.13	66
		b144	139	16 ± 3.2	0.19	45
		b182–1	123	21 ± 7.1	0.22	31
		b182–2	46	13 ± 3.0	0.13	9
		b182–3	323	15 ± 4.3	0.13	259
		b182–5	736	21 ± 5.7	0.12	327
5	26	c873–1	248	16 ± 2.0	0.18	262
		c873–2	491	18 ± 5.2	0.13	599
		c880–1	1327	22 ± 6.1	0.12	1730
		c880–2	317	16 ± 2.1	0.14	342
		c881	949	21 ± 4.2	0.10	1054
		c884–1	364	17 ± 2.3	0.14	189
		c884–2	88	17 ± 2.9	0.12	15
6	1	c932–1	422	12 ± 2.6	0.20	583
		c932–2	330	16 ± 3.3	0.18	342
		c929	582	12 ± 2.4	0.12	718
		c937–1	107	21 ± 3.2	0.17	28
		c937–2	286	21 ± 3.1	0.18	121
		c923	100	22 ± 4.2	0.18	20
6	44	9518	736	36 ± 2.7	0.16	373
		9524–1	357	35 ± 3.5	0.15	86
		9524–2	1203	33 ± 4.0	0.18	892
		9526–1	180	34 ± 7.1	0.14	25
		9526–2	304	40 ± 8.6	0.17	68
		9526–3	1363	35 ± 6.5	0.19	1114

[a]Mean value ±1 s standard deviation.

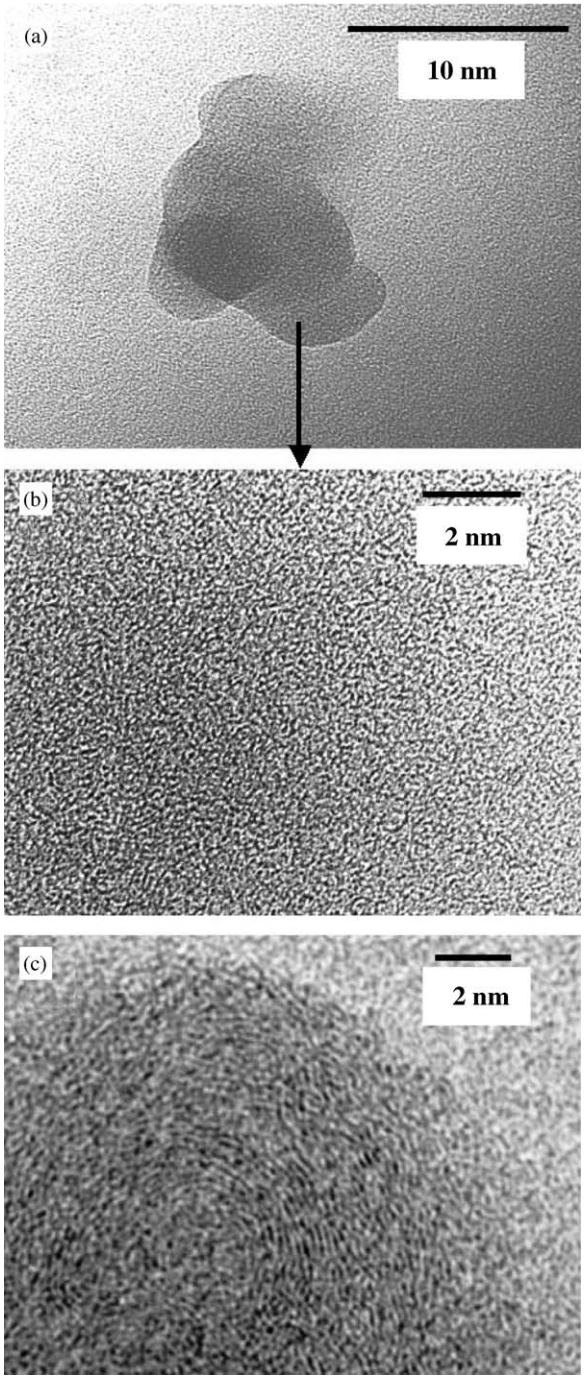

Fig. 2. TEM images of Palas soot. (a) Agglomerate of primary particles. (b) Amorpheous primary particle. (c) Primary particle consisting of nanocrystalline graphite with onion-shell structure.

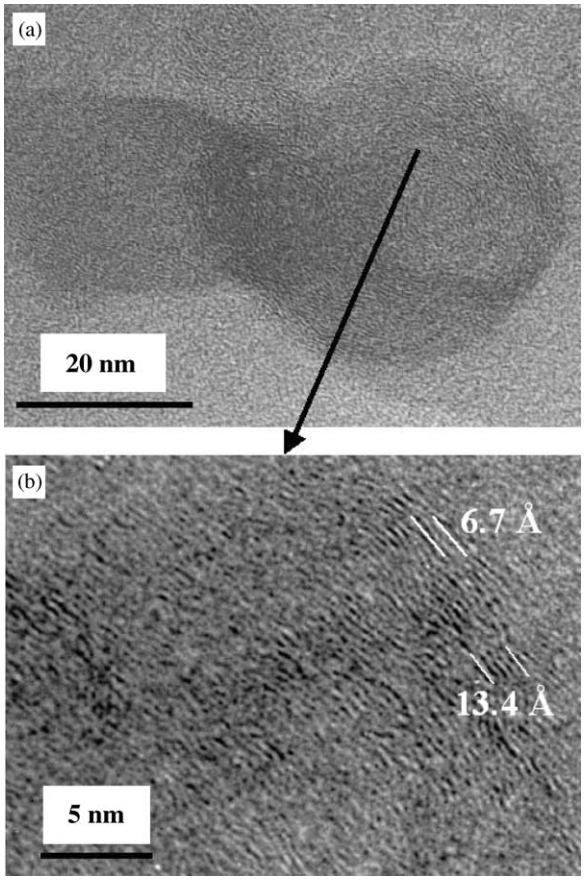

Fig. 3. TEM images of Diesel soot. (a) Agglomerate of primary particles consisting of nanocrystalline graphite with onion-shell structure. (b) Enlarged view of the onion-shell structure.

samples is currently not yet understood. An artifact from sampling or sample preparation can be certainly excluded. The small amounts of sulfur (< 1–2 wt%) detected in Diesel soot can be explained by the sulfur content of the fuel (383 mg/kg).

3.2. Fractal properties of soot agglomerates

The morphology of Palas and of Diesel soot agglomerates was studied by TEM. Bright-field images showing the typical chain-like soot agglomerates are given in Fig. 5. In total, the morphology of 37 Diesel soot agglomerates (from experiments # 2, # 5 and # 6) with the number of primary particles varying between 9 and 1730 was studied quantitatively. Using the approach of Brasil et al. (1999), the projected maximum length L_a, the mean primary particle diameter d_p, the overlap coefficient C_{ov} and the number of primary particles N_p were determined for each agglomerate (Table 1). For each sample, the fractal dimension D_{fL} and the fractal pre-factor k_L (Table 2) were deduced from the slope and intercept, respectively, of the straight line obtained in a double-logarithmic plot of

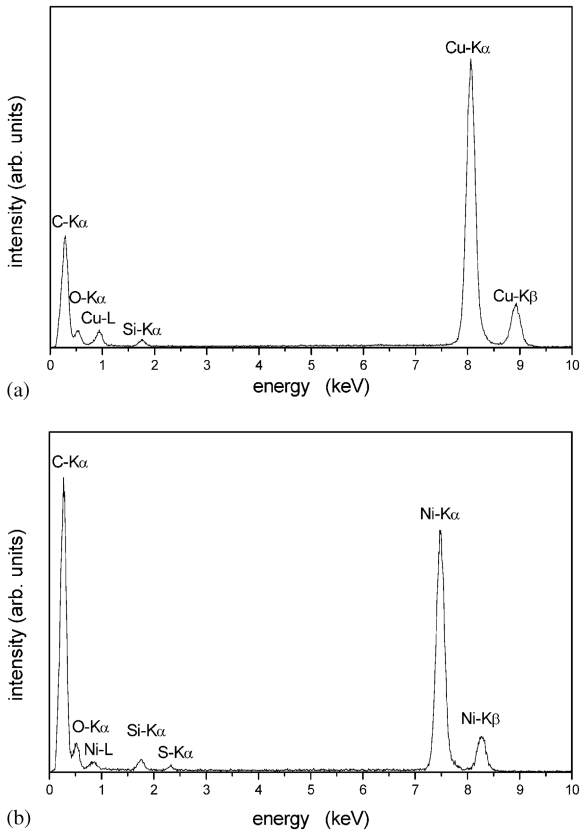

Fig. 4. Energy-dispersive X-ray spectra of (a) Palas soot and (b) Diesel soot.

N_p versus L_a/d_p (two examples are given in Fig. 6). The number of agglomerates used in the linear regression analysis varied between five and seven. The fractal dimension D_f and the fractal pre-factor k_g (Table 2) were derived from a double logarithmic plot of N_p versus R_g/r_p. We decided to determine D_f and k_g directly (i.e., not from Eqs. (3) and (4)) in order to estimate the errors in a similar way to those of D_{fL} and k_L. The fractal dimensions D_f of Diesel soot agglomerates obtained this way vary between 1.6 and 1.9 (Table 2). This is exactly the range of fractal dimensions reported previously in experimental (image analysis and light scattering of different combustion soots) and computational studies (see, e.g., the recent review by Brasil, Farias, & Carvalho, 2000). The average value determined from experiments #2, #5, and #6 is $D_f = 1.70 \pm 0.13$. The values of the fractal pre-factor k_g encountered in the AIDA campaign (1.9–4.1) are within the limits of error (see Table 2) identical to those reported in the literature (1.0–3.5; Brasil et al., 2000).

The fractal dimension of individual agglomerates was also determined using the nested squares method. The results for the individual agglomerates are given in Table 3, the mean values for each sample in Table 2. For illustration of this analysis procedure, a plot of $\ln N_{sq}$ versus $\ln l_{sq}$ is shown in Fig. 7 for two agglomerates. Pronounced deviations of the data points from a straight line can be seen. In principle, this may indicate that even the morphology of individual agglomerates is not

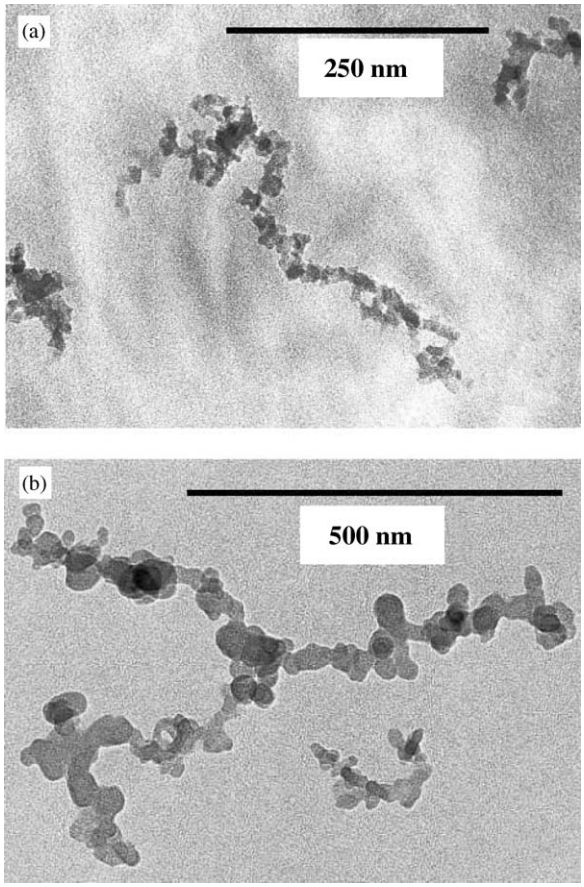

Fig. 5. TEM images of the typical chain-like agglomerates of (a) Palas soot and (b) Diesel soot.

Table 2
Fractal dimension and fractal pre-factors k_L and k_g of Diesel soot agglomerates derived from TEM using the approach of Brasil et al. (1999) and the nested-squares method

Experiment	Time (h)	n[a]	D_f and D_{fL}[b] Brasil et al. (1999)	k_L[b] Brasil et al. (1999)	k_g[b]	D_f[bc] nested squares
2	3	7	1.67 ± 0.10	1.91 ± 1.30	3.76 ± 1.24	1.44 ± 0.11
2	45	5	1.68 ± 0.27	1.37 ± 2.14	2.70 ± 1.92	1.44 ± 0.12
5	3	6	1.58 ± 0.13	1.48 ± 1.40	2.82 ± 1.33	1.26 ± 0.19
5	26	7	1.89 ± 0.20	0.90 ± 1.87	1.93 ± 1.73	1.41 ± 0.11
6	1	6	1.56 ± 0.10	2.15 ± 1.34	4.05 ± 1.29	1.32 ± 0.11
6	44	6	1.83 ± 0.08	1.35 ± 1.25	2.84 ± 1.21	1.55 ± 0.10

[a]Number of agglomerates.
[b]Mean value ± 1 standard error of the mean.
[c]Calculated for each sample from the data given in Table 3.

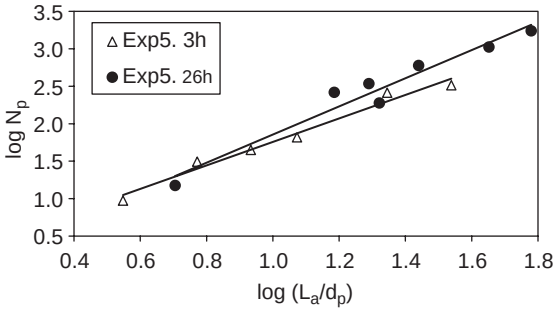

Fig. 6. Double logarithmic plot of the number of primary particles versus normalized projected maximum length of Diesel soot agglomerates yielding fractal dimension D_{fL} and fractal pre-factor k_L (using the method of Brasil et al., 1999).

Table 3
Fractal dimension D_f of individual Diesel soot agglomerates determined by the nested-squares method

Agglomerate	D_f[a]	Agglomerate	D_f[a]
Experiment #2; 3 h		Experiment #2; 45 h	
973	1.67 ± 0.12	c087	1.58 ± 0.07
978	1.80 ± 0.05	c146	1.57 ± 0.08
979	1.45 ± 0.09	c148	1.38 ± 0.05
981	0.93 ± 0.02	c153	1.00 ± 0.10
b613	1.21 ± 0.09	c156	1.66 ± 0.06
b617	1.61 ± 0.05		
b618	1.42 ± 0.05		
Experiment #5; 3 h		Experiment #5; 26 h	
b142	1.72 ± 0.06	c873–1	1.66 ± 0.06
b144	1.62 ± 0.03	c873–2	1.70 ± 0.11
b182–1	0.71 ± 0.01	c880–1	1.37 ± 0.08
b182–2	0.90 ± 0.09	c880–2	1.33 ± 0.04
b182–3	1.73 ± 0.17	c881	1.68 ± 0.09
b182–5	0.89 ± 0.02	c884–1	0.87 ± 0.08
		c884–2	1.27 ± 0.11
Experiment #6; 1 h		Experiment #6; 44 h	
c932–1	1.25 ± 0.09	9518	1.66 ± 0.01
c932–2	1.46 ± 0.08	9524–1	1.22 ± 0.01
c929	1.78 ± 0.09	9524–2	1.48 ± 0.03
c937–1	0.96 ± 0.06	9526–1	1.47 ± 0.07
c937–2	1.15 ± 0.07	9526–2	1.93 ± 0.01
c923	1.34 ± 0.02	9526–3	1.52 ± 0.02

[a]Mean value ±1 standard error of the mean.

appropriately described by a single fractal dimension. However, it is more likely that the deviations are an artifact of the analysis procedure (e.g., Katrinak et al., 1993). If the primary particles are not distributed homogeneously around the center of mass of the agglomerate, deviations from a straight

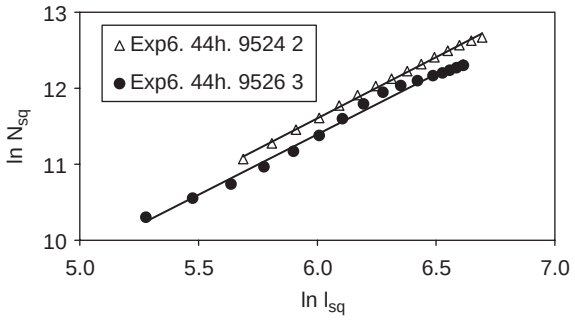

Fig. 7. Double logarithmic plot of N_{sq} versus l_{sq} yielding the fractal dimension of individual agglomerates of Diesel soot (using the nested squares method, e.g., Katrinak et al., 1993).

line may result. In addition, if the square length approaches pixel size, substantial deviations from a straight line are observed (e.g., Katrinak et al., 1993). The large variation of the fractal dimension of individual agglomerates from the same sample (Table 3) most likely results from the limitations of the nested-squares method outlined above.

The fractal dimension D_f obtained for an ensemble of aggregates using the approach of Brasil et al. (1999) is systematically higher than the mean value of the same group of agglomerates obtained by the nested sqaures method (Table 2). The difference between the two techniques of fractal analysis varies between 0.23 and 0.48, the mean difference is 0.31. According to Tence et al. (1986), the nested-squares method underestimates the true fractal dimension due to the finite size of the aggregates. The systematic error is on the order of 0.3 for $D_f = 2$ (Tence et al., 1986). This value is in excellent agreement with the mean difference (0.31) between the two approaches observed in this study. Hence, it can be concluded that the approach of Brasil et al. (1999) yields more accurate values for the fractal dimension than the nested-squares method.

Nevertheless, both methods seem to indicate an increasing fractal dimension of Diesel soot with time during the experiments #5 and #6 (mixture with ammonium sulfate), in contrast to experiment #2 (pure soot aerosol) where D_f remained constant. This could be explained by considering that the dynamics of the soot particles are most likely governed by a distribution of fractal dimensions rather than by a single value of D_f. The coagulation rate between fractal-like soot and compact ammonium sulfate particles increases with decreasing D_f, potentially resulting in an increasing average fractal dimension of the pure soot mode with time due to enhanced coagulation losses of the fraction of particles characterised by low D_f values. However, since our analysis is based on a limited number of agglomerates (6–7 per case, see Table 2) and the differences obtained by the method of Brasil et al. (1999) of $D_f(26\,h)$–$D_f(3\,h) = 0.31 \pm 0.33$ (experiment #5) and $D_f(44\,h)$–$D_f(1\,h) = 0.27 \pm 0.18$ (experiment #6) are very close to the errors, the statistical uncertainty of our results is too large to allow for an unambiguous verification of the hypothesis outlined above.

3.3. Mixing state of ammonium sulfate/soot mixtures

The mixing state of soot and ammonium sulfate has been studied in samples from experiments #5 and #6. According to TEM three different particle types can be distinguished: soot agglomerates

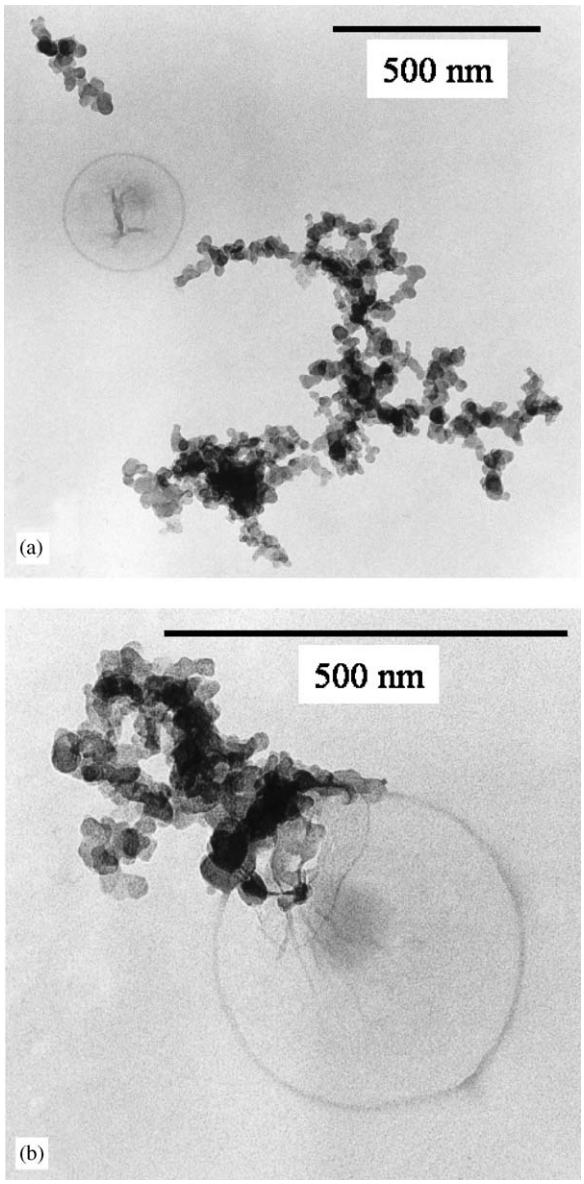

Fig. 8. TEM images of soot and ammonium sulfate mixtures: (a) Soot agglomerates and large individual particle of ammonium sulfate. The bright sphere is the residue of the sublimated sulfate particle. (b) Mixed particle consisting of an ammonium sulfate particle and a soot agglomerate. The bright sphere is the residue of the sublimated sulfate particle.

(Fig. 8a), spherical individual particles of ammonium sulfate (Fig. 8a) and mixed particles consisting of one (in most cases) ammonium sulfate particle and one to several soot agglomerates (Fig. 8b). The morphology of soot agglomerates is similar in all experiments, i.e., the fractal parameters D_f and k_g do not significantly depend on the concentration of soot or on the presence of an additional component (ammonium sulfate). The ammonium sulfate particles are quite large (mostly between

200 and 800 nm) compared to soot primary particles. In the mixed particles, soot is always found on the surface of ammonium sulfate (Fig. 8b). In contrast to atmospheric samples (Buseck & Posfai, 1999; Posfai et al., 1999; Posfai & Molnar, 2000; Gorzawski et al., 1999; Ebert et al., 2002), soot was never found as inclusion within ammonium sulfate particles. This result is not surprising, as the relative humidity was always $< 50\%$, well below the deliquesence point of ammonium sulfate.

The relative abundance of the three different particle types could not be determined quantitatively, as we have only investigated the outer regions of the impactor stages, in order to avoid sampling artifacts. At the center of the impacor stages too many particles were deposited to exclude agglomerate growth on the substrate during sampling. However, the change of the relative abundance of the different particle types with time can be deduced qualitatively. In both experiments (#5 and #6) the relative abundance of soot agglomerates increases with time, whereas the relatitive abundance of ammonium sulfate particles decreases. This observation can be easily explained by the preferential sedimentation of ammonium sulfate. Mixed particles consisting of soot and ammonium sulfate are frequently observed in all samples. The relative abundance of this particle type is on the order of some tens of a percent (10–40% by number) and increases with time.

The hetero-coagulation of fractal soot agglomerates and compact ammonium sulfate particles results in a dependence of the fractal dimension D_f on time and composition. Since the current version of the COSIMA code is limited to systems with constant fractal dimension, no results of model calculations can be given here.

3.4. Computer simulations on the dynamics of soot aerosols

Computer simulations on the dynamics of airborne Diesel and Palas soot have been performed using the aerosol behavior code COSIMA for conditions reflecting experiments #2 and #3, respectively. Together with the experimental data the numerical results are visualized in Figs. 9a and b for Diesel soot and in Figs. 10a and b for Palas soot. Since the light extinction of fractal-like soot particles in the UV-VIS region is to a very good approximation proportional to their mass concentration (Dobbins, Mulholland, & Bryner, 1994; Schnaiter et al., 2003), this information is included in Figs. 9a and 10a to supplement the filter samples which could be taken only at the beginning and at the end of the experiments. The optimum structural parameters obtained by comparing measured and calculated time evolutions of mass and number concentrations and of mobility-based size distributions are given in Table 4. They agree closely with the ones derived from estimating the mass concentration from the initial mobility size distribution as a function of D_f. Therefore, the latter are not listed separately.

During the initial phase of both experiments, aerosol dynamics is dominated by rapid coagulation resulting in a sharp decrease of number concentration and significant particle growth. This effect is more pronounced in the case of Palas soot because experiment #3 was started with somewhat higher mass and about an order of magnitude higher number concentration compared to experiment #2. Furthermore, the primary particles of Palas soot are much smaller than those of Diesel soot. Since both aerosols are characterized by the same fractal dimension, this results in a larger collisional cross-section for a given particle mass in the case of Palas soot. The evolutions of mass concentration and light extinction, on the other hand, solely reflect the impact of sedimentational deposition and particle diffusion to the chamber wall, since dilution due to sampling by the various instruments was negligible most of the time due to the large volume of the AIDA

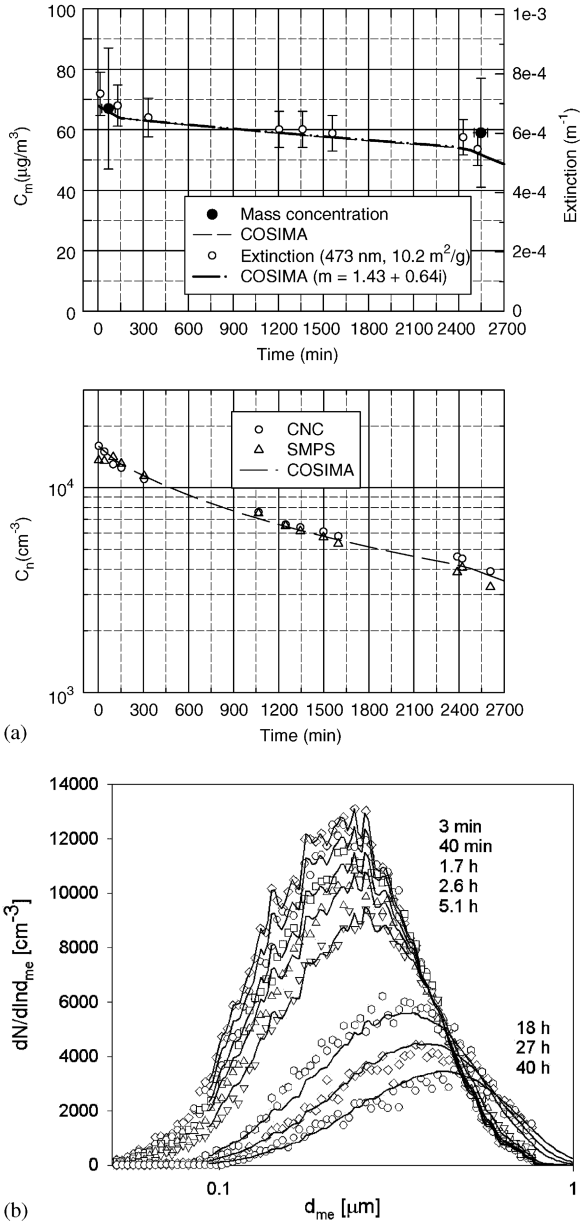

Fig. 9. Comparison of experimental (symbols) and COSIMA simulation (lines) results for Diesel soot. (a) Time evolution of extinction, mass and number concentration. (b) Time evolution of mobility-based size distribution.

facility. Only the steps at the beginning and at the end of the experiments are due to extensive sampling which, of course, is also accounted for by COSIMA. Clearly, only the time evolution of the mass concentration is suited to estimate the airborne residence time of concentrated agglomerate aerosols. Owing to the low diffusivity of highly ramified structures the observed half-lives

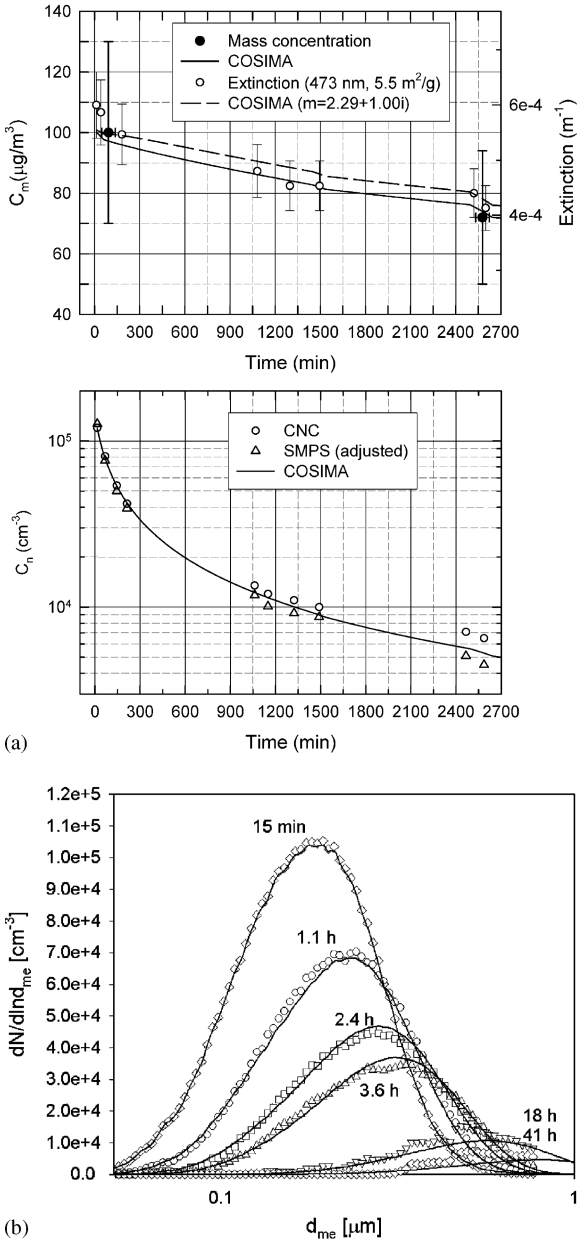

Fig. 10. Same as Fig. 9 for Palas soot. The prominent steps in the size distributions for 18 and 41 h are experimental artifacts resulting from inadequate correction for multiple charging of very large particles.

are more than twice as large for Diesel soot aerosol and more than four times as large for Palas soot, respectively, compared to ensembles of ideally spherical compact particles with a similar mass distribution.

Table 4
Optimum structural parameters for Diesel and Palas soot used with COSIMA simulations of aerosol dynamics. Overlap between primary particles can be approximately accounted for in case of Diesel soot

	Diesel soot[a] (overlap excluded)	Diesel soot[a] (overlap included)	Palas soot[a] (overlap excluded)
C_{ov}	0	0.15	0
D_f	2.0 ± 0.1	1.9 ± 0.2	2.0 ± 0.1
$2r_p$ (nm)	27 ± 3	25 ± 3	7.3 ± 0.8
f	1.43	1.05	1.43
ρ (kg/m^3)[b]	1700	1700	2000

[a]Error margins reflect the experimental uncertainties only.
[b]Bulk material density (values assumed and not varied during the fitting procedure).

3.5. Comparison of TEM image analysis and COSIMA modeling results

The algorithm currently implemented in COSIMA is based on the assumption that the fractal dimension D_f is independent of particle size and, therefore, does not vary as a result of coagulation events. The good agreement between calculated and observed size distribution evolutions for both Diesel and Palas soot over periods of 2 days lends credit to this idea. Additional support comes from the fractal analysis of the TEM images of samples collected during experiment #2 after 3 and 45 h which showed no indications for significant changes in D_f. The comparison of our numerical and experimental results thus provides evidence that coagulation in pure Diesel and Palas soot aerosols exhibiting atmospherically relevant particle sizes is not accompanied by restructuring.

Regarding the determination of the structural parameters for Diesel and Palas soot, the comparison of calculated and measured time evolutions of mobility size distribution, mass and number concentration proved to be an efficient procedure. Very good agreement between simulation and experiment and unambiguous results for D_f and r_p could be obtained. For both experiments under consideration (#2 and #3) we found unique optimum solutions for D_f and r_p while other combinations of these parameters gave more or less inferior results. The average primary particle diameters $2r_p$ obtained this way are 27 ± 3 nm for Diesel soot and 7.3 ± 0.8 nm for Palas soot, respectively, thus comparing favorably with the TEM image analysis (Figs. 1a and b). We would like to recall here, however, that the COSIMA model assumes equally sized primary particles in contrast to size distributions encountered in reality. The close correspondence between measured and numerical results observed in this study as well as in earlier applications (e.g., Kamm, Möhler, Naumann, Saathoff, & Schurath, 1999; Möhler et al., 1994) indicates that the use of mean values, while significantly simplifying the model, does not seriously affect the quality of the simulations. This is practically important, since TEM image analysis required to determine the size distribution of primary particles in fractal-like agglomerates cannot be considered a routine aerosol-analytical tool yet.

By analyzing the mobility size distributions for Palas soot obtained during the early phases of experiment #9, prior to coating with oxidation products of α-pinene, the value of 7.3 nm for the average primary particle diameter could be confirmed and is, therefore, assumed to be representative for all Palas soot experiments during our campaign. Interestingly, it is somewhat larger than the

value of 5 nm given in the reference study by Helsper et al. (1993) but consistent with the value reported earlier by Schwyn, Garwin, and Schmidt-Ott (1988) for a carrier gas flow velocity matching our experimental conditions. Correspondingly, the specific surface area of our Palas soot was determined to $308 \pm 30\ m^2/g$ by N_2-thermodesorption spectroscopy (O. Popovitcheva, Moscow State University, personal communication) opposed to the BET value of $395\ m^2/g$ measured by Helsper et al. (1993).

The volume fractal dimension D_f delivered by the computer simulation approach is 2.0 ± 0.1 for both Diesel and Palas soot, suggesting a certain structural similarity which is also apparent from the TEM micrographs (Figs. 5a and b). Inserting this value into Eq. (8), the fractal prefactor is calculated to $k_g = 1.4 \pm 0.02$, close to the value obtained from the diffusion limited cluster–cluster aggregation model (Brasil et al., 2000).

For Palas soot our result $D_f = 2.0 \pm 0.1$ closely agrees with the value 2.1 reported by Weingartner, Baltensperger, and Burtscher (1995). They employed an in situ technique combining a differential mobility analyzer with a low pressure impactor (Schleicher, Künzel, & Burtscher, 1995). This combination of mobility and aerodynamic sizing bears a certain resemblance to our procedure. On the other hand, Mikhailov et al. (2001) recently published values of 1.63 ± 0.08 and 1.72 ± 0.15, respectively, obtained from two different methods of TEM image analysis which, however, could both potentially result in too low D_f values, as noted by the authors themselves. A similar discrepancy appears to emerge in the case of Diesel soot. The average fractal dimension derived from our TEM image analysis, 1.70 ± 0.13, is hardly compatible with the value 2.0 ± 0.1 obtained from the computer simulation approach. Since the optimum parametrization of the COSIMA model is very sensitive to the time evolution of the mobility size distribution, it could be suspected that there is a principal discrepancy between methods relying on differential mobility sizing and methods based on the fractal analysis of TEM images. However, it will be shown below that this presumption is not supported by our results.

For agglomerate aerosols obeying free molecular particle dynamics the following trivial explanation would be obvious. Ramified structures with volume fractal dimensions below 2 are more or less transparent, i.e. their accessible surface has reached its maximum value. Therefore, decreasing D_f below 2 does not significantly enhance the drag excerted on the particles by the carrier gas (Schmidt-Ott, Baltensperger, Gäggeler, & Jost, 1990). As a result, mobility measuring devices will be insensitive to fractal dimensions below 2 under free molecular conditions. However, for Diesel soot the mean mobility equivalent diameter was around 200 nm during the early stages of experiment #2, and around 500 nm after 40 h. In the case of Palas soot, this quantity increased from about 200 nm to circa 550 nm. Comparing these values to the mean free pathlength of the carrier gas molecules of about 70 nm, it becomes obvious that our experiments were initialized well within the transition regime, passing over to almost continuum conditions during the later stages. Therefore, it would have been possible in principle to detect fractal dimensions below 2 from mobility sizing measurements. Furthermore, performing COSIMA simulations with $D_f < 2$ results in increased particle growth due to enhanced coagulation since the collisional cross-section of the particles increases with decreasing D_f. As a result, the calculated size distributions are shifted away from the measured ones spoiling the good agreement between experiment and theory. The same holds true for the time evolution of the number concentration.

Another possible reason for the discrepancy between TEM image analysis and the computer simulation approach regarding the value of D_f is related to the fact that partial overlap between primary

particles is neglected in the standard version of the COSIMA model. Inspecting our TEM images of Diesel soot agglomerates, however, such overlap has been undoubtedly detected with an average overlap coefficient C_{ov} of about 0.15 (Table 1). Overlap between monomers leads to more compact agglomerate structures accompanied by increased particle mobility. In model calculations neglecting overlap effects, this has to be compensated for by assuming a slightly larger fractal dimension D_f.

Extending the Kirkwood–Riseman theory (Kirkwood & Riseman, 1948; Doi & Edwards, 1986), a basic ingredient of the COSIMA formalism, to account for overlap between monomers is by no means a trivial task and was not attempted in this study. It is nevertheless possible to give an estimate on the effect of including overlap into the model. Following Oh and Sorensen (1997), we assume that Eq. (1) remains valid for clusters made up of overlapping primary particles. Then, with N_p, D_f, and r_p kept constant one has $k_g(C_{ov}) * R_g^{D_f}(C_{ov}) = \text{const.}$, as well as $k_g(0) * R_g^{D_f}(0) = \text{const.}$ Brasil, Farias, Carvalho, and Käylü (2001) found empirically $R_g(C_{ov}) = R_g(0) * (1 - C_{ov})$. Combining these results leads to

$$k_g(C_{ov}) = \frac{k_g(0)}{(1 - C_{ov})^{D_f}}. \tag{9}$$

Inserting this result into Eq. (8), it immediately follows

$$f(C_{ov}) = f(0)(1 - C_{ov})^{D_f}. \tag{10}$$

The mass m_2 of two overlapping spherical monomers is given by

$$m_2 = \frac{4\pi r_p^3}{3} \rho[1 + 1.5(1 - C_{ov}) - 0.5(1 - C_{ov})^3]. \tag{11}$$

Assuming an average coordination number c and neglecting multiple overlap (i.e., only overlap in pairs is considered) it follows from Eq. (11)

$$m_{N_p}(C_{ov}) = m_{N_p}(0) \left[1 - \{1 - 1.5(1 - C_{ov}) + 0.5(1 - C_{ov})^3\} \frac{c}{2}\right]. \tag{12}$$

The same scaling also applies to the mass concentration c_m. From Fig. 5 of Brasil et al. (2001), the average coordination number is about 2.5 for clusters of fractal dimension 1.82. Adopting this value for our numerical studies and substituting Eqs. (10) and (12) for f and c_m the COSIMA simulations were repeated. With $C_{ov} = 0.15$ the optimum parameters changed to $D_f = 1.9 \pm 0.2$ and $2r_p = 25 \pm 3$ nm, the increased error margin for D_f reflecting the experimental as well as the methodological uncertainties in the determination of C_{ov} documented in Table 1 and in Eq. (3) of (Brasil et al. 1999), respectively. Thus, by accounting for overlap between adjacent monomers simulation results and TEM data are reconciled in the case of Diesel soot.

For Palas soot, we were not able to reliably determine the fractal dimension D_f and the overlap coefficient C_{ov} from our TEM images. In order to estimate the potential overlap effect on the COSIMA parameterisation for Palas soot, the simulations were repeated assuming the same average C_{ov}-value as measured for Diesel soot ($C_{ov} = 0.15$) as a first guess. Thereby, the optimum value for

D_f reduced to 1.9, which lies between the values of 1.6–1.7 observed by Mikhailov et al. (2001) and 2.1 reported by Weingartner et al. (1995). However, applying a projectional distortion correction, which was neglected by Mikhailov et al. (2001), would most likely shift their results towards higher values for D_f as explicitly admitted by the authors themselves, bringing them potentially into close mutual agreement with the corrected COSIMA predictions.

A potential problem associated with the analysis of mobility size distributions as performed in this study and by Weingartner et al. (1995) is the proper correction for multiple particle charging. As the total surface of a fractal particle is larger than that of a mobility equivalent compact sphere, the charge distribution routinely used in the inversion procedure may not be adequate. Higher charging would shift the corrected size distribution towards larger diameters resulting in a lower fractal dimension when compared to mass concentration measurements. Unfortunately, this effect cannot be quantified at present. Clearly, additional work is necessary to further improve the consistency between mobility analysis and TEM image analysis.

4. Conclusions

Combining TEM and first principle computer simulation techniques, the particle structure and aerosol dynamics of Diesel and Palas soot and of mixtures of Diesel soot with ammonium sulfate have been investigated. Both soots exhibit a fractal-like agglomerate structure which does not undergo significant compaction during coagulation. Palas soot mainly consists of amorphous carbon, but nanocrystalline graphitic domains were also observed in a few cases. The average diameter of the monomers is around 7 nm. The primary particles of Diesel soot always show a typical onion-shell structure, their average size being 23 nm and the average overlap coefficient around 0.15. TEM shows that the initially external mixture of Diesel soot and ammonium sulfate developed with time in a significant degree of internal mixing.

The semi-empirical scheme proposed by Brasil et al. (1999) to determine the fractal dimension of agglomerates from electron micrographs has been successfully applied in practice for the first time. It was found to be superior to the nested-squares method which systematically underestimates the value of D_f. The average fractal dimension derived from TEM image analysis of Diesel soot particles is 1.70 ± 0.13.

Our computer simulations using the fractal–aerosol behavior code COSIMA closely reproduced the measured time evolutions of the mobility size distributions, mass, and number concentrations over the complete experiment time of 2 days for both soot types. The code can, thus, be considered a reliable tool for predicting the dynamics of airborne agglomerate particles as well as for the analysis of experimental data. The average primary particle diameters obtained from the model analysis are in perfect agreement with the TEM observations. A fractal dimension D_f of 1.9 ± 0.2 (overlap correction included) is obtained for Diesel soot, and 2.0 ± 0.1 (no overlap correction) for Palas soot. It is concluded that within the experimental error limits both approaches (TEM image analysis and COSIMA simulation) are consistent.

Acknowledgements

This work has been funded by BMBF under grant 07AF209/5. The authors would like to acknowledge the engaged technical assistance of the whole AIDA staff.

References

Brasil, A. M., Farias, T. L., & Carvalho, M. G. (1999). A recipe for image characterization of fractal-like aggregates. *Journal of Aerosol Science*, *30*, 1379–1389.

Brasil, A. M., Farias, T. L., & Carvalho, M. G. (2000). Evaluation of the fractal properties of cluster-cluster aggregates. *Aerosol Science and Technology*, *33*, 440–454.

Brasil, A. M., Farias, T. L., Carvalho, M. G., & Köylü, Ü. O. (2001). Numerical characterization of the morphology of aggregated particles. *Journal of Aerosol Science*, *32*, 489–508.

Buseck, P. R., & Posfai, M. (1999). Airborne minerals and related aerosol particles: Effects on climate and the environment. *Proceedings of the National Academy of Sciences, USA*, *96*, 3372–3379.

Cachier, H. (1998). Carbonaceous combustion aerosols. In R. M. Harrison, & R. Van Grieken (Eds.), *Atmospheric Particles* (pp. 295–348). Chichester: Wiley.

Cai, J., Lu, N., & Sorensen, C. M. (1995). Analysis of fractal cluster morphology parameters: Structural coefficient and density autocorrelation function cutoff. *Journal of Colloid and Interface Science*, *171*, 470–473.

Cooke, W. F., Liousse, C., Cachier, H., & Feichter, J. (1999). Construction of a 1 degrees × 1 degrees fossil fuel emission data set for carbonaceous aerosol and implementation and radiative impact in the ECHAM4 model. *Journal of Geophysical Research D*, *104*, 22 137–22 162.

Dobbins, R. A., Mulholland, G. W., & Bryner, N. P. (1994). Comparison of a fractal smoke optics model with light extinction measurements. *Atmospheric Environment*, *28*, 889–897.

Doi, M., & Edwards, S. F. (1986). *The theory of polymer dynamics*. Oxford: Clarendon Press.

Dye, A. L., Rhead, M. M., & Trier, C. J. (2000). The quantitative morphology of roadside and background urban aerosol in Plymouth, UK. *Atmospheric Environment*, *34*, 3139–3148.

Ebert, M., Weinbruch, S., Rausch, A., Gorzawski, G., Hoffman, P., Wex, H., & Helas, G. (2002). The complex refractive index of aerosols during LACE 98 as derived from the analysis of individual particles. *Journal of Geophysical Research*, *Journal of Geophysical Research—Atmospheres*, *107* (D21), 8121, doi:10.1029/2000JD000195, LAC 3-1-LAC 3-15.

Forrest, S. R., & Witten, T. A. (1979). Long-range correlation in smoke particle aggregates. *Journal of Physics*, *A12*, L109–L117.

Gorzawski, G., Rausch, A., Ebert, M., Weinbruch, S., Hoffmann, P., & Helas, G. (1999). Elemental and phase composition of aerosols sampled during LACE 98. *Journal of Aerosol Science*, *30*, S517–S518.

Helsper, C., Mölter, W., Löffler, F., Wadenpohl, C., Kaufmann, S., & Wenninger, G. (1993). Investigation of a new aerosol generator for the production of carbon aggregate particles. *Atmospheric Environment*, *27A*, 1271–1275.

Huang, P.-F., Turpin, B. J., Piho, M. J., Kittelson, D. B., & McMurry, P. H. (1994). Effects of water condensation and evaporation on diesel chain-agglomerate morphology. *Journal of Aerosol Science*, *25*, 447–459.

Intergovernmental Panel on Climate Change, (IPCC) (2001). Contribution of working group I to the third assessment report: Climate change 2001: The scientific basis. In J. T. Houghton, Y. Ding, D. J. Griggs, M. Noguer, P. J. van der Linden, & D. Xiaosu (Eds.), Cambridge, MA: Cambridge University Press.

Jacobson, M. Z. (2001). Strong radiative heating due to the mixing state of black carbon in atmospheric aerosols. *Nature*, *409*, 695–697.

Kamm, S., Möhler, O., Naumann, K.-H., Saathoff, H., & Schurath, U. (1999). The heterogeneous reaction of ozone with soot aerosol. *Atmospheric Environment*, *33*, 4651–4661.

Katrinak, K. A., Rez, P., Perkes, P. R., & Buseck, P. R. (1993). Fractal geometry of carbonaceous aggregates from an urban aerosol. *Environmental Science and Technology*, *27*, 539–547.

Kaye, B. H. (1994). *A random walk through fractal dimensions* (2nd ed.). Weinheim: Verlag Chemie.

Kirkwood, J. G., & Riseman, J. (1948). The intrinsic viscosities and diffusion constants of flexible macromolecules in solution. *Journal of Chemical Physics*, *16*, 565–573.

Köylü, Ü. O., Faeth, G. M., Farias, T. L., & Carvalho, M. G. (1995a). Fractal and projected structure properties of soot aggregates. *Combustion and Flame*, *100*, 621–633.

Köylü, Ü. O., Xing, Y., & Rosner, D. E. (1995b). Fractal morphology analysis of combustion-generated aggregates using angular scattering and electron microscope images. *Langmuir*, *11*, 4848–4854.

Lesaffre, F. (1989). Characterization of aerosol aggregates through fractal parameters. Effects due to humidity. *Journal of Aerosol Science*, *20*, 857–860.

Mikhailov, E. F., Vlasenko, S. S., Krämer, L., & Niessner, R. (2001). Interaction of soot aerosol particles with water droplets: Influence of surface hydrophilicity. *Journal of Aerosol Science*, *32*, 697–711.

Möhler, O., Naumann, K.-H., & Schöck, W. (1994). Dynamic behaviour of fractal soot aerosols. *Journal of Aerosol Science*, *25*, S303–S304.

Naumann, K.-H. (2003). COSIMA—a computer program simulating the dynamics of fractal aerosols. *Journal of Aerosol Science*, *34*, 1371–1397.

Naumann, K.-H., & Bunz, H. (1991). Aerodynamic properties of fractal aerosol particles. *Journal of Aerosol Science*, *22*, S161–S164.

Naumann, K.-H., & Bunz, H. (1992). Computer simulations on the dynamics of fractal aerosols. *Journal of Aerosol Science*, *23*, S361–S364.

Oh, C., & Sorensen, C. M. (1997). The effect of overlap between monomers on the determination of fractal cluster morphology. *Journal of Colloid and Interface Science*, *193*, 17–25.

Posfai, M., Anderson, J. R., & Buseck, P. R. (1999). Soot and sulfate aerosol particles in the remote marine troposphere. *Journal of Geophysical Research*, *104*(D17), 21 685–21 693.

Posfai, M., & Molnar, A. (2000). Aerosol particles in the troposphere: A mineralogical introduction. In D. J. Vaughan, R. A. Wogelius (Eds.), *Environmental mineralogy* (pp. 197–252). Budapest: Eötvös University Press.

Saathoff, H, Möhler, O., Schurath, U., Kamm, S., Dippel, B., & Mihelcic, D. (2003). The AIDA soot aerosol characterisation campaign 1999. *Journal of Aerosol Science*, *34*, 1277–1296.

Samson, R. J., Mulholland, G. W., & Gentry, J. W. (1987). Structural analysis of soot agglomerates. *Langmuir*, *3*, 272–281.

Schleicher, B., Künzel, S., & Burtscher, H. (1995). In situ measurement of size and density of submicron aerosol particles. *Journal of Applied Physics*, *78*, 4416–4422.

Schmidt-Ott, A., Baltensperger, U., Gäggeler, H. W., & Jost, D. T. (1990). Scaling behaviour of physical parameters describing agglomerates. *Journal of Aerosol Science*, *21*, 711–717.

Schnaiter, M., Horvath, H., Möhler, O., Naumann, K.-H., Saathoff, H., Schöck, W., & Schurath, U. (2003). UV-VIS-NIR spectral optical properties of soot containing aerosols. *Journal of Aerosol Science*, *34*, 1421–1444.

Schwyn, S., Garwin, E., & Schmidt-Ott, A. (1988). Aerosol generation by sparc discharge. *Journal of Aerosol Science*, *19*, 639–642.

Seinfeld, J. H., & Pandis, S. N. (1998). *Atmospheric chemistry and physics: From air pollution to climate change*. New York: Wiley.

Sorensen, C. M., & Feke, G. D. (1996). The morphology of macroscopic soot. *Aerosol Science and Technology*, *25*, 328–337.

Tence, M., Chevalier, J. P., & Jullien, R. (1986). On the measurement of the fractal dimension of aggregated particles by electron microscopy: Experimental method, corrections and comparison with numerical models. *Journal de Physique*, *47*, 1989–1998.

Weingartner, E., Baltensperger, U., & Burtscher, H. (1995). Growth and structural change of combustion aerosol at high relative humidity. *Environmental Science and Technology*, *29*, 2982–2986.

Wieser, P., & Wurster, R. (1986). Application of laser-microprobe mass analysis to particle collections. In K. R. Spurny (Ed.), Physical and chemical characterization of individual airborne particles (pp. 251–270). Chichester: Ellis Horwood Ltd.

Wu, M., & Friedlander, S. K. (1993). Note on the power law equation for fractal-like aerosol agglomerates. *Journal of Colloid and Interface Science*, *159*, 246–248.

Zhang, H. X., Sorensen, C. M., Ramer, E. R., Olivier, B. J., & Merklin, J. F. (1988). In situ optical structure factor measurements of an aggregating soot aerosol. *Langmuir*, *4*, 867–871.